

Compatibility Analysis of Multi-Sensor Vegetation Indices Using EO-1 Hyperion Data

T. Miura^{a,*}, J. Tsend-Ayush^a, J. P. Turner^a

^aDepartment of Natural Resources and Environmental Management, College of Tropical Agriculture and Human Resources, University of Hawaii at Manoa, Honolulu, HI 96822, USA – (tomoakim, javzan, turnerjp)@hawaii.edu

Abstract – In this study, we used a set of hyperspectral Hyperion scenes and assessed the effects of differing spectral and spatial resolutions on MODIS-AVHRR vegetation index (VI) continuity. Hyperion scenes were processed to simulate atmospherically-corrected normalized difference vegetation index (NDVI) and 2-band enhanced vegetation index (EVI2) values at MODIS Climate Modeling Grid (CMG) and AVHRR Global Area Coverage (GAC) resolutions. Our analysis of their differences suggests that MODIS CMG and AVHRR GAC VIs can be combined to generate a long-term data record, but would be accompanied by added uncertainties due to scaling differences.

Keywords: NDVI, EVI, EVI2, Continuity, Scaling Uncertainty, Hyperion, MODIS, AVHRR, VIIRS

1. INTRODUCTION

Numerous satellite optical sensors have been launched and planned for launch for monitoring and characterization of the Earth system and its behaviors. These sensors have been providing and will continue to provide systematic observations of terrestrial vegetation at various spatial, spectral, and temporal resolutions. Spectral vegetation indices (VIs) are among the most widely used satellite data products in monitoring temporal and spatial variations of vegetation photosynthetic activities and biophysical properties. Although they are not intrinsic physical quantities, VIs are widely used as proxies in the assessments of many canopy state and biophysical process variables, including leaf area index, fraction of absorbed photosynthetically-active radiation, vegetation fraction, and gross primary production (e.g., Myneni, Nemani, & Running, 1997; Sims et al., 2008).

Utilities of these observations greatly increase when datasets from multiple sensors are combined, e.g., multi-decadal land cover characterization and change detection via multi-sensor data sources (e.g., Bhattarai, Conway, & Yousef, 2009; Jepson, Brannstrom, & Filippi, 2010; Paudel & Andersen, 2010), synergistic applications of multi-resolution remote sensing for forest and rangeland inventory (e.g., DeFries et al., 2007; Miettinen & Liew, 2009), and a development of multi-sensor, long-term data records for climate studies (Yu, Privette, & Pinheiro, 2005; Tucker et al., 2005; Pedelty et al., 2007).

Applications of multi-sensor observations, however, require consideration and account of continuity and compatibility due to differences in sensor/platform characteristics (Teillet, Staenz, & Williams, 1997; Batra, Islam, Venturini, Bisht, & Jiang, 2006). One key sensor characteristic that varies widely among sensors is the spectral bandpass filters and many previous studies have focused on this “spectral” issue (e.g., Trishchenko, Cihlar, & Li, 2002). Another key sensor characteristic that varies across sensors is spatial resolution (point spread

function, PSF). Although it is critical, the spatial issue of continuity has not been paid as much attention as the spectral issue (e.g., Chen, 1999).

Hyperspectral remote sensing has great potential in addressing these key issues of multi-sensor VI continuity and providing deeper insights and understanding of them. An ultimate advantage of using hyperspectral remote sensing for multi-sensor continuity studies is that it allows to analyze the effects of multiple factors individually and simultaneously (Teillet et al., 1997). Current and future hyperspectral sensors provide medium resolution images (3 – 100 m spatial resolution with 30 m being typical) with swaths of 3 – 150 km with 30 km being typical. These resolutions are fine enough and these swath widths are wide enough to allow to simulate various pixel footprint sizes via spatial aggregation. The aggregated data can be used to examine VI compatibility across multiple resolutions (Huete, Ho-Jin, & Miura, 2005).

In this study, we assessed the effects of spectral bandpass and spatial resolution differences on cross-sensor VI continuity. Specifically, we analyzed inter-sensor compatibility between AVHRR Global Area Coverage (GAC) and MODIS Climate Modeling Grid pixels for two indices, the Normalized Difference Vegetation Index (NDVI) (Tucker, 1979) and 2-band Enhanced Vegetation Index (EVI2) (Jiang, Huete, Didan, & Miura, 2008) using hyperspectral data obtained with Earth Observing-One (EO-1) Hyperion (Ungar, Pearlman, Mendenhall, & Reuter, 2003). Our particular interest was to assess scaling uncertainties that would arise in absence and presence of spectral bandpass differences.

2. MATERIALS

Five study sites were selected within the conterminous United States (Table 1), based upon availability of nearly cloud-free Hyperion scenes, availability of *in situ* atmospheric measurements from the Aerosol Robotic Network (AERONET) (Holben et al., 2001), and a diversity of land cover types. Level 1R Hyperion scenes were obtained for the 5 sites for the dates listed in Table 1. For each Hyperion scene, Level 2 AERONET data were acquired for a two hour time period bracketing the image acquisition time (\pm one hour).

Hyperion images were spectrally-convolved to spectral bandpasses of the Terra MODIS and NOAA-14 AVHRR sensors and converted to top-of-atmosphere (TOA) reflectances. The spectral response curves of these satellite sensors were splined to Hyperion band center wavelengths for each Hyperion pixel (Miura, Huete, & Yoshioka, 2006) as every Hyperion pixel had a slightly different spectral calibration (spectral smile) (Pearlman et al., 2003).

These spectrally-convolved Hyperion TOA reflectance scenes were spatially convolved to MODIS 500 m and AVHRR 1.1

* Corresponding author.

** This work was supported partially by a NASA contract, NNX08AT05A.

km resolutions. We assumed a triangular and bell-shaped PSF in the scan direction for MODIS and AVHRR, respectively, and a rectangular PSF in the track direction for both MODIS and AVHRR (Wolfe et al., 2002; Schowengerdt, 2006). The latter data were further averaged to produce GAC pixels. A GAC pixel value represents the mean of four out of each five consecutive samples along the scan line (Pinheiro, Mahoney, Privette, & Tucker, 2006).

These spectrally- and spatially-convolved images were corrected for atmosphere with the “6S” radiative transfer code (Vermote et al., 2006). The 6S radiative transfer code was constrained with scene specific geometric conditions extracted from the corresponding image metadata and *in situ* AERONET atmospheric data. The continental aerosol model was assumed for all the aerosol corrections, based on the aerosol model selection criteria described in Kaufman et al. Kaufman et al. (1997). After the atmospheric corrections, the simulated MODIS 500 m resolution data were spatially aggregated into CMG pixels (5 km-by-5 km).

The two VIs, NDVI and EVI2, were computed from the atmospherically-corrected CMG and GAC resolution data

$$NDVI = \frac{\rho_{NIR} - \rho_{red}}{\rho_{NIR} + \rho_{red}}, \quad (1)$$

$$EVI2 = 2.5 \frac{\rho_{NIR} - \rho_{red}}{\rho_{NIR} + 2.4\rho_{red} + 1}, \quad (2)$$

where ρ_{NIR} and ρ_{red} are the NIR and red reflectances. The EVI2 equation have been optimized to achieve the best similarity with the original, 3-band EVI and is applicable to sensors without a blue band (Jiang et al., 2008).

3. METHODS

Central to VI spatial compatibility is the scale-invariance properties or scaling uncertainties of VIs under the influence of land surface heterogeneity (Hall, Huemmrich, Goetz, Sellers, & Nickeson, 1992; Friedl, Davis, Michaelsen, & Moritz, 1995; Hu & Islam, 1997; Chen, 1999). Below, we compare the finer and coarser resolution VIs using the NDVI as an example.

The fine grain NDVI can be aggregated to a coarser resolution pixel by (Hu & Islam, 1997; Huete et al., 2005)

$$\begin{aligned} NDVI_{fine} &= f_1 \cdot NDVI_1 + f_2 \cdot NDVI_2 \\ &= \frac{f_1 \cdot (\rho_{NIR,1} - \rho_{red,1})}{\rho_{NIR,1} + \rho_{red,1}} + \frac{f_2 \cdot (\rho_{NIR,2} - \rho_{red,2})}{\rho_{NIR,2} + \rho_{red,2}}, \end{aligned} \quad (3)$$

where two surface types with the fractional amounts of f_1 and f_2 ($f_1 + f_2 = 1$) are assumed. This quantity is not generally equal to the coarser resolution NDVI computed from the reflectances at the resolution analyzed, which can be expressed using the fine grain reflectances as

$$\begin{aligned} NDVI_{coarse} &= \frac{(f_1 \cdot \rho_{NIR,1} + f_2 \cdot \rho_{NIR,2}) - (f_1 \cdot \rho_{red,1} + f_2 \cdot \rho_{red,2})}{(f_1 \cdot \rho_{NIR,1} + f_2 \cdot \rho_{NIR,2}) + (f_1 \cdot \rho_{red,1} + f_2 \cdot \rho_{red,2})}, \quad (4) \\ &= \frac{f_1 \cdot (\rho_{NIR,1} - \rho_{red,1}) + f_2 \cdot (\rho_{NIR,2} - \rho_{red,2})}{f_1 \cdot (\rho_{NIR,1} + \rho_{red,1}) + f_2 \cdot (\rho_{NIR,2} + \rho_{red,2})} \end{aligned}$$

and, thus,

$$NDVI_{coarse} \neq NDVI_{fine} \text{ or } D \equiv NDVI_{coarse} - NDVI_{fine} \neq 0. \quad (5)$$

These two quantities are equal, or the quantity D is equal to zero (1) when either f_1 or f_2 is equal to zero (i.e., homogeneous case) (Huete et al., 2005) or (2) when the 1-norms of the two endmember spectra are equal (i.e., $\rho_{NIR,1} + \rho_{red,1} = \rho_{NIR,2} + \rho_{red,2}$)

(Hu & Islam, 1997). Theoretically, at least, the former also applies to the EVI2 formula (Huete et al., 2005).

To assess scaling uncertainties between GAC and CMG pixels, five of GAC pixels were averaged to generate fine-grain VI values approximately equal to the CMG pixel size. These spatial aggregations and averaging of Hyperion pixels were performed carefully and systematically so that the derived fine-grain GAC and coarse-grain CMG pixels were co-located without mis-registration.

4. RESULTS

In Figs. 1a and 1b, only the effect of the spectral bandpass difference between Terra MODIS and NOAA-14 AVHRR on the NDVI and EVI2, respectively, was assessed for the two spatial resolutions. MODIS-AVHRR cross-sensor NDVI and EVI2 relationships for the GAC resolution were basically the same as those for the CMG resolution, i.e., the trends in the relationships were the same for the two resolutions.

In Figs. 1c and 1d, only the effects of the spatial resolution difference between the CMG and GAC resolutions (scaling uncertainties) was assessed for the NDVI and EVI2, respectively, by fixing the spectral bandpasses. There were large variations in scale-induced differences for all the four cases (MODIS NDVI, AVHRR NDVI, MODIS EVI2, and AVHRR EVI2), ranging from -.05 to .05 at most for MODIS NDVI (Fig. 1c); however, these scaling uncertainties did not appear to introduce any systematic differences (i.e., mean differences ≈ 0).

In Figs. 1e and 1f, the combined effects of the spectral bandpass and spatial resolution differences between MODIS CMG and AVHRR GAC VIs were assessed for the NDVI and EVI2, respectively. For both the NDVI and EVI2, the trends in cross-sensor relationships remained similar to those due only to the spectral bandpass difference; however, the secondary scattering about the mean trends became larger due to the scale-induced variations. These results suggest that MODIS CMG and AVHRR GAC VIs can be combined to generate a long-term data record, but would be accompanied by added uncertainties due to scaling differences.

5. DISCUSSIONS

The assessment conducted in this study can be expanded to a larger dataset to obtain more reliable estimates of scaling uncertainties. We also plan to evaluate how well GAC pixels (1 km-by-5 km) represent CMG grids (5 km-by-5 km) and the impact of no aerosol correction on AVHRR-MODIS continuity.

REFERENCES

- Batra, N., Islam, S., Venturini, V., Bisht, G., & Jiang, L. (2006). Estimation and comparison of evapotranspiration from MODIS and AVHRR sensors for clear sky days over the Southern Great Plains. *Remote Sensing of Environment*, 103(1), 1-15.
- Bhattarai, K., Conway, D., & Yousef, M. (2009). Determinants of deforestation in Nepal's central development region. *Journal of Environmental Management*, 91(2), 471-488.
- Chen, J. M. (1999). Spatial scaling of a remotely sensed surface parameter by contexture. *Remote Sensing of Environment*, 69(1), 30-42.
- DeFries, R., Achard, F., Brown, S., Herold, M., Murdiyarso, D., Schlamadinger, B., & de, S. J., Carlos. (2007). Earth

- observations for estimating greenhouse gas emissions from deforestation in developing countries. *Environmental Science & Policy*, 10(4), 385-394.
- Friedl, M. A., Davis, F. W., Michaelsen, J., & Moritz, M. A. (1995). Scaling and uncertainty in the relationship between the NDVI and land surface biophysical variables: An analysis using a scene simulation model and data from FIFE. *Remote Sensing of Environment*, 54(3), 233-246.
- Hall, F. G., Huemmrich, K. F., Goetz, S. J., Sellers, P. J., & Nickeson, J. E. (1992). Satellite remote sensing of surface energy balance: Success, failures, and unresolved issues in FIFE. *Journal of Geophysical Research*, 97(D17), 19061-19089.
- Holben, B. N., Tanré, D., Smirnov, A., Eck, T. F., Slutsker, I., Abuhassan, N., Newcomb, W. W., Schafer, J. S., Chatenet, B., Lavenu, F., Kaufman, Y. J., Vande Castle, J., Setzer, A., Markham, B., Clark, D., Frouin, R., Halthore, R., Karneli, A., O'Neill, N. T., Pietras, C., Pinker, R. T., Voss, V., & Zibordi, G. (2001). An emerging ground-based aerosol climatology: Aerosol Optical Depth from AERONET. *Journal of Geophysical Research*, 106, 12,067-12,097.
- Hu, Z., & Islam, S. (1997). A framework for analyzing and designing scale invariant remote sensing algorithms. *IEEE Transactions on Geoscience and Remote Sensing*, 35(3), 747-755.
- Huete, A., Ho-Jin, K., & Miura, T. (2005). Scaling dependencies and uncertainties in vegetation index - biophysical retrievals in heterogeneous environments. *Proceedings of IGARSS '05*, 7, 5029-5032.
- Jepson, W., Brannstrom, C., & Filippi, A. (2010). Access regimes and regional land change in the Brazilian Cerrado, 1972-2002. *Annals of the Association of American Geographers*, 100(1), 87-111.
- Jiang, Z., Huete, A. R., Didan, K., & Miura, T. (2008). Development of a two-band enhanced vegetation index without a blue band. *Remote Sensing of Environment*, 112(10), 3833-3845.
- Kaufman, Y. J., Tanré, D., Remer, L. A., Vermote, E. F., Chu, A., & Holben, B. N. (1997). Operational remote sensing of tropospheric aerosol over land from EOS moderate resolution imaging spectroradiometer. *Journal of Geophysical Research*, 102(D14), 17051-17067.
- Miettinen, J., & Liew, S. C. (2009). Estimation of biomass distribution in Peninsular Malaysia and in the islands of Sumatra, Java and Borneo based on multi-resolution remote sensing land cover analysis. *Mitigation and Adaptation Strategies for Global Change*, 14(4), 357-373.
- Miura, T., Huete, A., & Yoshioka, H. (2006). An empirical investigation of cross-sensor relationships of NDVI and red/near-infrared reflectance using EO-1 Hyperion data. *Remote Sensing of Environment*, 100(2), 223-236.
- Myneni, R. B., Nemani, R. R., & Running, S. W. (1997). Estimation of global leaf area index and absorbed par using radiative transfer models. *IEEE Transactions on Geoscience and Remote Sensing*, 35(6), 1380-1393.
- Paudel, K. P., & Andersen, P. (2010). Assessing rangeland degradation using multi temporal satellite images and grazing pressure surface model in Upper Mustang, Trans Himalaya, Nepal. *Remote Sensing of Environment*, 114(8), 1845-1855.
- Pearlman, J. S., Barry, P. S., Segal, C. C., Shepanski, J., Beiso, D., & Carman, S. L. (2003). Hyperion, a space-based imaging spectrometer. *IEEE Transactions on Geoscience and Remote Sensing*, 41(6), 1160-1173.
- Pedelty, J., Devadiga, S., Masuoka, E., Brown, M., Pinzon, J., Tucker, C., Roy, D., Junchang, J., Vermote, E., Prince, S., Nagol, J., Justice, C., Schaaf, C., Jicheng, L., Privette, J., & Pinheiro, A. (2007). Generating a long-term land data record from the AVHRR and MODIS Instruments. *IGARSS 2007*, 1021-1025.
- Pinheiro, A. C. T., Mahoney, R., Privette, J. L., & Tucker, C. J. (2006). Development of a daily long term record of NOAA-14 AVHRR land surface temperature over Africa. *Remote Sensing of Environment*, 103(2), 153-164.
- Schowengerdt, R. A. (2006). *Remote Sensing: Models and Methods for Image Processing* (Third ed.). Academic Press.
- Sims, D. A., Rahman, A. F., Cordova, V. D., El-Masri, B. Z., Baldocchi, D. D., Bolstad, P. V., Flanagan, L. B., Goldstein, A. H., Hollinger, D. Y., Misson, L., Monson, R. K., Oechel, W. C., Schmid, H. P., Wofsy, S. C., & Xu, L. (2008). A new model of gross primary productivity for North American ecosystems based solely on the enhanced vegetation index and land surface temperature from MODIS. *Remote Sensing of Environment*, 112(4), 1633-1646.
- Teillet, P. M., Staenz, K., & Williams, D. J. (1997). Effects of spectral, spatial, and radiometric characteristics on remote sensing vegetation indices of forested regions. *Remote Sensing of Environment*, 61(1), 139-149.
- Trishchenko, A. P., Cihlar, J., & Li, Z. (2002). Effects of spectral response function on surface reflectance and NDVI measured with moderate resolution satellite sensors. *Remote Sensing of Environment*, 81(1), 1-18.
- Tucker, C. J. (1979). Red and photographic infrared linear combinations for monitoring vegetation. *Remote Sensing of Environment*, 8(2), 127-150.
- Tucker, C. J., Pinzon, J. E., Brown, M. E., Slayback, D. A., Pak, E. W., Mahoney, R., Vermote, E. F., & El, S., Nazmi. (2005). An extended AVHRR 8-km NDVI dataset compatible with MODIS and SPOT vegetation NDVI data. *International Journal of Remote Sensing International Journal of Remote Sensing*, 26(20), 4485-4498.
- Ungar, S. G., Pearlman, J. S., Mendenhall, J. A., & Reuter, D. (2003). Overview of the Earth Observing One (EO-1) mission. *IEEE Transactions on Geoscience and Remote Sensing*, 41(6), 1149-1159.
- Vermote, E., Tanré, D., Deuzé, J. L., Herman, M., Morcrette, J. J., & Kotchenova, S. Y. (2006). *Second Simulation of a Satellite Signal in the Solar Spectrum - Vector (6SV) User Guide Version 3*.
- Wolfé, R. E., Nishihama, M., Fleig, A. J., Kuyper, J. A., Roy, D. P., Storey, J. C., & Patt, F. S. (2002). Achieving sub-pixel geolocation accuracy in support of MODIS land science. *Remote Sensing of Environment*, 83(1-2), 31-49.
- Yu, Y. Y., Privette, J. L., & Pinheiro, A. C. (2005). Analysis of the NPOESS VIIRS land surface temperature algorithm using MODIS data. *IEEE Transactions on Geoscience and Remote Sensing*, 43(10), 2340-2350.

ACKNOWLEDGEMENTS

We thank the PIs of the five AERONET sites used in this study for their effort in establishing and maintaining these sites.

Table 1. List of Study Sites, Hyperion Image Properties

Geographic Location	Latitude / Longitude	Biome Type	Date (yyyy/mm/dd)	θ_s / θ_v^a (degrees)
Harvard Forest, MA	42.532° / -72.188°	Broadleaf Forest	2001/09/05	40.5 / 3.6
			2008/05/07	32.2 / 12.1
			2008/05/25	28.5 / 4.8
			2008/05/30	28.6 / 12.8
			2008/06/07	26.2 / 10.1
2008/12/03	67.1 / 5.2			
Walker Branch, TN	35.958° / -84.287°	Broadleaf Forest	2001/08/14	31.3 / 2.3
Maricopa, AZ	33.069° / -111.972°	Broadleaf Cropland / Open Shrubland	2001/05/24	23.3 / 5.5
			2001/07/27	26.4 / 5.4
			2001/08/28	32.3 / 5.0
			2001/12/02	58.6 / 4.6
2001/12/18	60.5 / 4.7			
Konza Prairie, KS	39.102° / -96.610°	Prairie Grassland / Cereal Crop	2002/10/19	52.3 / 2.6
			2009/05/08	29.4 / 1.3
Sevilleta, NM	34.355° / -106.885°	Semi-arid Grassland / Open Shrubland / Cereal Crop	2001/10/19	48.8 / 5.0
			2009/01/16	61.5 / 16.9
			2009/09/25	40.8 / 4.3
			2009/10/05	45.2 / 18.6
			2009/11/05	54.2 / 12.1
2009/12/06	60.8 / 5.7			

a – θ_s : solar zenith angle, θ_v : view zenith angle

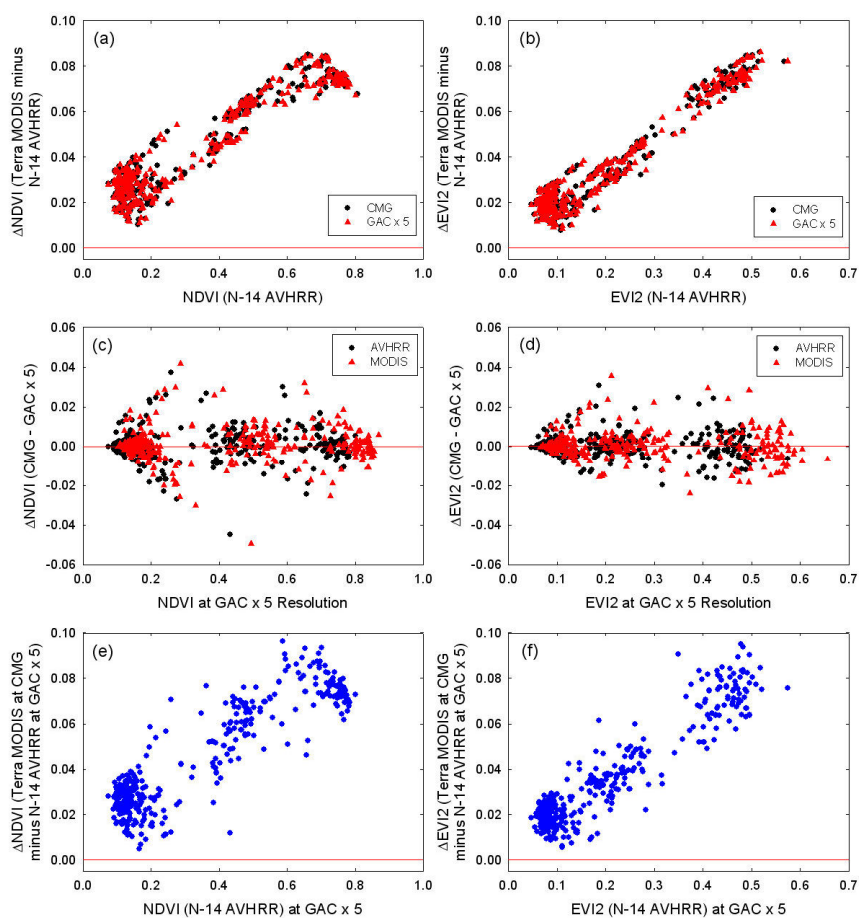


Fig. 1. (a) NDVI and (b) EVI2 differences due to spectral bandpass differences for CMG and GAC resolutions; (c) NDVI and (d) EVI2 differences due to spatial resolution differences for AVHRR and MODIS spectral bandpasses; (e) NDVI and (f) EVI2 differences due to both spectral bandpass (MODIS vs. AVHRR) and spatial resolution (CMG vs. GAC) differences. Here, a GAC pixel is an average of five GAC pixels and, thus, written as “GAC x 5”.